MINIMUM ENERGY ANALYSIS OF MEMBRANE DEFORMATION APPLIED TO PIPET ASPIRATION AND SURFACE ADHESION OF RED BLOOD CELLS

EVAN A. EVANS, *Department of Biomedical Engineering, Duke University, Durham, North Carolina 27706 U.S.A.*

ABSTRACT An experimental procedure is demonstrated which can be used to determine the interfacial free energy density for red cell membrane adhesion and membrane elastic properties. The experiment involves micropipet aspiration of a flaccid red blood cell and manipulation of the cell proximal to a surface where adhesion occurs. A minimum free energy method is developed to model the equilibrium contour of unsupported membrane regions and to evaluate the partial derivatives of the total free energy, which correspond to the micropipet suction force and the interfacial free energy density of adhesion. It is shown that the bending elasticity of the red cell membrane does not contribute significantly to the pressure required to aspirate a flaccid red cell. Based on experimental evidence, the upper bound for the bending or curvature elastic modulus of the red cell membrane is 10^{-12} ergs (dyn-cm). Analysis of the adhesion experiment shows that interfacial free energy densities for red cell adhesion can be measured from a lower limit of 10^{-4} ergs/cm^2 to an upper limit established by the membrane tension for lysis of 5–10 ergs/cm^2.

INTRODUCTION

Mechanical experiments have demonstrated that the red blood cell membrane can store energy in a conservative manner; this elastic solid behavior is limited by the magnitude and duration of applied forces (see Evans and Hochmuth, 1978; Evans and Skalak, 1980, for general review). The significant feature of the mechanical behavior is that the resistance to area change is four to five orders of magnitude greater than resistance to in-plane extensional (shear) deformation; bending rigidity or resistance to curvature change is usually an even lower magnitude contribution. Thus, nonspherical cells are very flaccid and easily deformed by membrane extension and curvature changes at constant surface area. Elastic deformations of the red cell are related to the forces applied to the cell through a compliance factor which involves the shear and bending elastic moduli and the cell shape. If the compliance factor can be determined, the deformation of the red cell provides a direct measure of the forces that act on the cell in static equilibrium. In other words, the red cell can be used as a "force transducer." This concept can be applied in the study of red cell adhesion to other cell surfaces or to artificial material surfaces. In this paper, an experimental procedure will be outlined for implementation of the concept and then the details of the analysis of the cell deformation will be developed based on thermodynamic equilibrium.

The equilibrium shape of the unsupported cell membrane contour is determined with a variational method based on the first law of thermodynamics for isothermal, reversible processes, i.e., the variation in the free energy of the membrane minus the variation in work of

surface tractions which act on the membrane equals zero. A similar variational approach has been developed by Zarda et al., 1977; their results have contributed significantly to the understanding of cell deformation in the microcirculation. However, there are some important differences between the approach taken by these authors and that to be presented here. Zarda et al. have used a finite element technique where the membrane is partitioned into sequential elements with several nodal positions inside each element. The positions of the nodes are defined by spatial coordinates, which are the radial and axial positions for the axisymmetric membrane surface. The free energy variations lead to integrals of membrane tension and moment resultants at the nodal positions multiplied by functions of the surface geometry; the integrands represent the equations of mechanical equilibrium for the membrane. Within each element, the tension and moment resultants plus the surface geometry are approximated by polynomials of the degree appropriate to the number of nodal positions; continuity at element interfaces is assured by adding constraint equations for element curvature at the interface. The requirement of surface incompressibility (i.e., constant local area) involves additional constraint equations. The result is a system of equations of very large dimensionality. In the approach to be described in this paper, the axisymmetric surface geometry is represented by intrinsic or curvilinear coordinates which are defined such that the first and second derivatives are continuous over the entire contour. Only the angular coordinate values at a few points on the contour and its derivatives at the ends are involved as free variables in the variational procedure. The first and second variations of the free energy functional are derived analytically; therefore, the integrands are continuous functions over the entire contour. In addition, nonlocal energy functionals are considered, specifically nonlocal bending or curvature energy variations. The variation of a nonlocal free energy integral does not simply become the integral of the variation of the free energy density (i.e., the variation of the integrand). Based on physical structure, for example, the bending elastic energy of a phospholipid bilayer is best represented by a nonlocal energy functional because its component layers can slip relative to each other (Evans, 1974; Evans and Skalak, 1980). On the other hand, a membrane with strongly associated material (like the peripheral protein structure of a red cell membrane) will be characterized by local and nonlocal bending energy functionals in addition to the shear elastic energy contribution.

Numerical solutions of the equations for mechanical equilibrium of a membrane with local elastic resistance to curvature and area changes have been obtained by Jenkins (1977). Even though the approach can be extended to include surface shear elasticity, the implementation is very difficult when auxiliary constraints are imposed, e.g., constant cell volume, fixed distance between bounding surfaces, etc. Also, nonlocal energy functionals usually make direct derivation of differential equations for equilibrium impossible.

EXPERIMENTAL PROCEDURE

As discussed in the introduction, the elastic character of the red cell membrane can be employed to measure static forces that act on the cell surface. Clearly, the elastic properties must be measured on the particular cell to "calibrate" the transducer, and the compliance relation between cell deformation and applied forces must be determined. The particular application to be considered in this paper is the adhesion of red cell membrane to an adjacent surface, e.g., another red cell membrane or a different cell surface or even an artificial

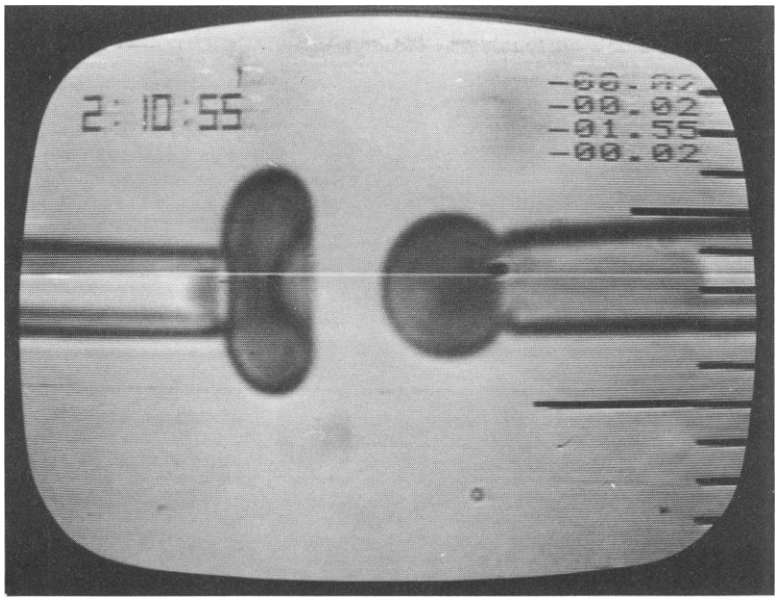

FIGURE 1 Photograph of a videorecording of two red blood cells, each aspirated with a suction micropipet. The flaccid cell on the left is aspirated with a negative pressure of $\sim 2 \times 10^2$ dyn/cm^2; the cell on the right is forced into a rigid spherical "test" surface with a negative pressure on the order of 10^4 dyn/cm^2. The micrometer scale on the right is $\sim 10^{-4}$ cm/division.

material surface. Fig. 1 shows an experimental method that incorporates the measurement of cell elastic compliance with the adhesion to an arbitrary "test" surface. Here, the elastic property and compliance of the cell are established by the displacement of the cell into a micropipet with a controlled aspiration pressure that can range from 10 to 100,000 dyn/cm^2; for a flaccid cell, the suction pressure is on the order of 100 dyn/cm^2. The "test" surface in this case is another red cell which has been aspirated with a sufficiently large pressure to form a rigid spherical portion outside the micropipet. Next, the micropipets are brought into close proximity without forcing the surfaces to contact (Fig. 2 *a*). The two pipets are left stationary at these two positions. Because of the Brownian motion of the flaccid cell membrane, eventually the membrane forms contact and adhesion occurs (Fig. 2 *b*). The waiting period is arbitrary and on the order of several seconds to a minute; contact is quickly completed (1–2 s) after the adhesion process commences. Since the micropipets are stationary, the forces at the support boundaries do no work. The long-range forces between the surfaces do work on the elastic membrane, deform the membrane into a new shape, and cause the cell projection in the pipet to be displaced. During the brief, time-dependent deformation before equilibrium, the excess work of the long-range forces between the surfaces is dissipated by viscous processes in the cell membrane and in the adjacent fluid phases. Equilibrium is established when the virtual change in energy of the interfacial contact is balanced by the virtual change in elastic energy of the membrane. Either the displacement of the cell membrane in the micropipet or the general shape of the cell membrane can be used to determine the work of the adhesion process per unit area of surface contact. The cell displacement in the pipet will be useful for adhesive energy densities (work per unit area) in the range of 5×10^{-3} to 5 ergs/cm^2; the

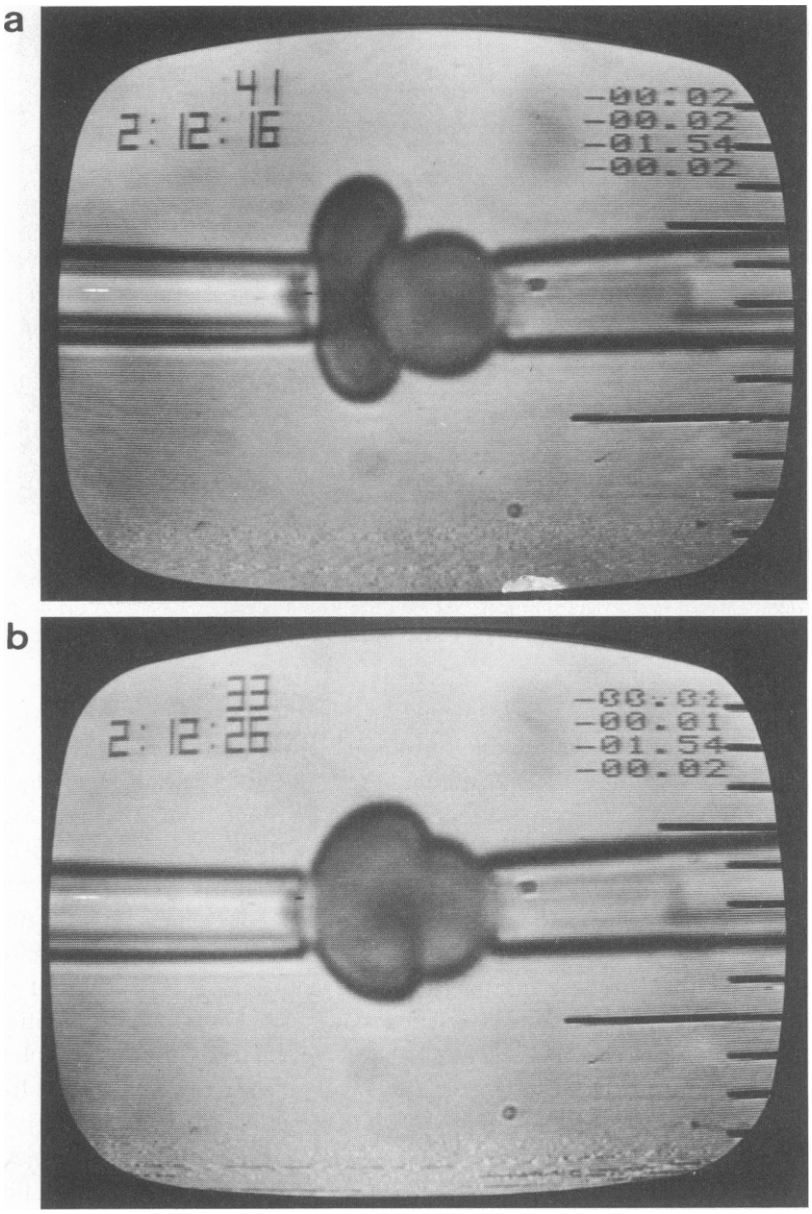

FIGURE 2 (*a*) The cells shown in Fig. 1 are brought into close proximity to each other and then left stationary. (*b*) After a few seconds to a minute, the membrane of the flaccid cell deforms and contacts the spherical cell surface; adhesion occurs. This particular case is mediated by a 3-gm-% dextran solution (150,000 mol wt), 150 mM ionic strength. Based on subsequent analysis, the interfacial free energy density for the work of adhesion is estimated to be 3×10^{-3} ergs/cm^2.

deformation state of the whole cell will be the appropriate indicator for the range of 10^{-4} to 5×10^{-3} ergs/cm^2. Skalak et al. (1977) (footnote 1) have modeled red cell rouleaux formation using their finite element approach and have demonstrated that the cell shape is useful for low values of energy density (10^{-4} to 10^{-3} ergs/cm^2); but for adhesion to a flat surface, which these authors have considered, the range of the characteristic cell dimension (specifically the major diameter) is very limited and difficult to detect because of optical diffraction.

WORK OF SURFACE TRACTIONS AND MEMBRANE EQUILIBRIUM

Many biologically significant reactions involve adhesive contact; these are mediated by a wide variety of agents, e.g., multivalent ligands (Nicholson, 1974; Bell, 1979), plasma proteins and expanders (Brooks, 1973; Chien, 1975), etc. These surface reactions (including the electrostatic and electrodynamic interactions of colloidal systems; see Israelachvilli, 1974, or Parsegian, 1975, for discussion) are really prominent only over short range compared with observable cellular dimensions (i.e., a few hundred ångströms). Thus, the details of the actual forces between the surfaces are not observable and are cumulated into an integral of force times displacement, i.e., the work involved in forming an adhesive contact. Since the surface radii of curvature are usually much larger than the distance between surfaces, the forces are distributed per unit surface area as a normal traction, σ_z; therefore, the work per unit area involved in formation of the adhesive contact is the integral relation,

$$\gamma = -\int_{\infty}^{z_c} \sigma_z \, dz, \tag{1}$$

where the contact position z_c refers to the equilibrium position for membrane surfaces that have adhered but have not necessarily established physical contact. The distance, z, is measured from a surface that is rigidly fixed to the displaced surface that is initially considered to be "far away."

Near the equilibrium state, the virtual work done on the cell capsule is the integral over the capsule of the surface tractions times the virtual displacement of the surface,

$$\delta W = \sum_{i=1}^{3} \int (\sigma_i \delta\zeta_i) dA, \tag{2}$$

where σ_i are the components of the traction which act on the surface and $\delta\zeta_i$ are the components of the local virtual displacement. Since only uniform pressure exists in the fluid phases, this integral can be expressed in terms of the external fluid pressure, P_o, the pressure in the pipet, P_p, and the interfacial energy density, γ, for the adhesion process, $\delta W = -P_o \int_o (\delta\zeta_n) dA - P_p \int_p (\delta\zeta_n) dA + \gamma \cdot \delta A_c$, where the integrals represent the cell segments outside and inside the pipet, respectively; $\delta\zeta_n$ is the displacement normal to the surface; and A_c is the interfacial contact area. (Friction at the pipet wall is assumed to be negligible.) It is recognized that the integrals are simply the virtual changes in the volumes of the cell segments outside and inside the pipet respectively, $\delta W = -P_o \cdot \delta V_o - P_p \cdot \delta V_p + \gamma \cdot \delta A_c$. Since the cellular contents are an incompressible liquid solution, these volume variations are equal but

[1]Skalak, R. Personal communication.

of opposite sign; thus, $\delta W = \Delta P \cdot \delta V_p + \gamma \cdot \delta A_c$, where $\Delta P \equiv P_o - P_p$. The variation of the volume in the pipet is given by the variation of the projection length, L, in the pipet, $\delta V_p = (\pi R_p^2)\delta L$, with R_p as the pipet radius. (This assumes that the projection length, L, is greater than the pipet radius, R_p, and that the shape of the projection cap is constant [e.g., a hemisphere].) Consequently, the variation in work is given simply by the virtual displacement of a pipet suction force and the interfacial energy density times the variation in contact area,

$$\delta W = (\pi R_p^2)\Delta P \cdot \delta L + \gamma \cdot \delta A_c. \tag{3}$$

For an isothermal, equilibrium process, the variation in work is equal to the variation in Helmholtz free energy of the system. Since the cytoplasm is an incompressible liquid, the free energy variation is the membrane free energy variation, δF; hence,

$$\delta F = \delta W = (\pi R_p^2)\Delta P \cdot \delta L + \gamma \cdot \delta A_c. \tag{4}$$

The isothermal free energy is an elastic (conservative) potential function which yields,

$$\left(\frac{\partial F}{\partial L}\right)_{A_c} = (\pi R_p^2)\Delta P, \tag{5}$$

$$\left(\frac{\partial F}{\partial A_c}\right)_{L} = \gamma, \tag{6}$$

and,

$$(\delta F)_{A_c,L} = 0. \tag{7}$$

These relations provide the analytical recipes for determining the pipet suction pressure and interfacial energy density of adhesion from the equilibrium deformations of the membrane. The last relation, Eq. 7, states that the unsupported membrane contour will be an extremum energy shape for specific values of contact area and projection length.

MINIMUM ENERGY ANALYSIS OF MEMBRANE DEFORMATION

To determine the contour that will minimize the membrane free energy, it is necessary to define a function of several variables, a_i, which describes the axisymmetric surface geometry; then, the membrane free energy is made stationary with respect to these variables. (For an excellent development of the methods of the calculus of variations, see Courant and Hilbert, 1966.) The free energy can be expressed in a Taylor series expansion about a location defined by a specific set of independent variables, $\bar{a}_i$; to second order, the expansion is,

$$F = F_0 + \sum_{i=1}^{N} \frac{\partial F}{\partial a_i}\bigg|_{\bar{a}_i} (a_i - \bar{a}_i) + \sum_{i=1}^{N}\sum_{j=1}^{N} \frac{1}{2}\frac{\partial^2 F}{\partial a_i \partial a_j}\bigg|_{\bar{a}_i,\bar{a}_j} (a_i - \bar{a}_i)(a_j - \bar{a}_j) + \cdots, \tag{8}$$

where the free energy, F_0, and its derivatives are evaluated at the location given by the set, $\bar{a}_i$, of N variables. If the location of a minimum is nearby, then Eq. 7 is satisfied by the simultaneous solution to the system of equations,

$$\frac{\partial F}{\partial a_i} = 0 = \frac{\partial F}{\partial a_i}\bigg|_{\bar{a}_i} + \sum_{j=1}^{N} \frac{\partial^2 F}{\partial a_i \partial a_j}\bigg|_{\bar{a}_i,\bar{a}_j} (a_j - \bar{a}_j) + \cdots, \tag{9}$$

where the location of the minimum is defined by the set of variables, a_i. Often a particular problem involves subsidiary or constraint conditions (e.g., the cell volume is constant because of incompressibility; the distance between the pipet entrance and the spherical surface held by the opposite pipet is fixed). In such cases, the system of equations is enlarged and the independent variable set will include a Lagrange multiplier, α_i, for each subsidiary condition, $G_i(a_j)$. Thus, Eq. 9 becomes,

$$G_i(a_j) \equiv 0$$

$$\frac{\partial F}{\partial a_i} + \sum_{k-1}^{N_c} \alpha_k \cdot \frac{\partial G_k}{\partial a_i} = 0, \tag{10}$$

which represents a system of $(N + N_c)$ equations in $(N + N_c)$ unknowns; N_c is the number of subsidiary conditions. With the definition of matrix and vector variables, the system of equations, (10), is written in terms of the appropriate summations to first order,

$$G_i = 0$$

$$0 = \bar{F}_i + \sum_{j-1}^{N} \bar{F}_{ij}(a_j - \bar{a}_j) + \sum_{k-1}^{N_c} \bar{G}_{ki}\alpha_k, \tag{11}$$

where,

$$\bar{F}_i \equiv \left.\frac{\partial F}{\partial a_i}\right|_{\bar{a}_i},$$

$$\bar{F}_{ij} \equiv \left.\frac{\partial^2 F}{\partial a_i \partial a_j}\right|_{\bar{a}_i,\bar{a}_j},$$

$$\bar{G}_{ki} \equiv \left.\frac{\partial G_k}{\partial a_i}\right|_{\bar{a}_i}.$$

The task now is to introduce the elastic free energy functional for the red cell membrane. As outlined in the introduction, experiments have shown that the red cell membrane has a great resistance to area dilation and much lower shear and bending rigidities. Thus, the red cell membrane can be treated as a two-dimensionally incompressible surface material, i.e., it deforms at constant area. As such, local deformations of membrane can be described by a single surface extension ratio, λ, and by changes in the principal curvatures, K_1 and K_2, that characterize the surface. Fig. 3 illustrates the deformation of an element of the axisymmetric membrane surface. Based on theoretical considerations, the first-order elastic free energy functional for the membrane is given by the superposition of shear and curvature elastic effects (Evans and Hochmuth, 1978; Evans and Skalak, 1980),

$$F = \underbrace{\int \frac{\mu}{2}(\lambda^2 + \lambda^{-2} - 2)\mathrm{d}A_0}_{\text{"Shear"}} + \underbrace{\int \frac{B}{2}(K_1 + K_2)^2 \mathrm{d}A_0}_{\text{"Bending"}}$$

$$+ \underbrace{\int \Gamma(K_1 + K_2)\mathrm{d}A_0}_{\text{"Chemical"}} + \underbrace{\frac{\bar{B}}{2}\left|\int (K_1 + K_2)\mathrm{d}A_0\right|^2}_{\text{"Nonlocal bending"}},$$

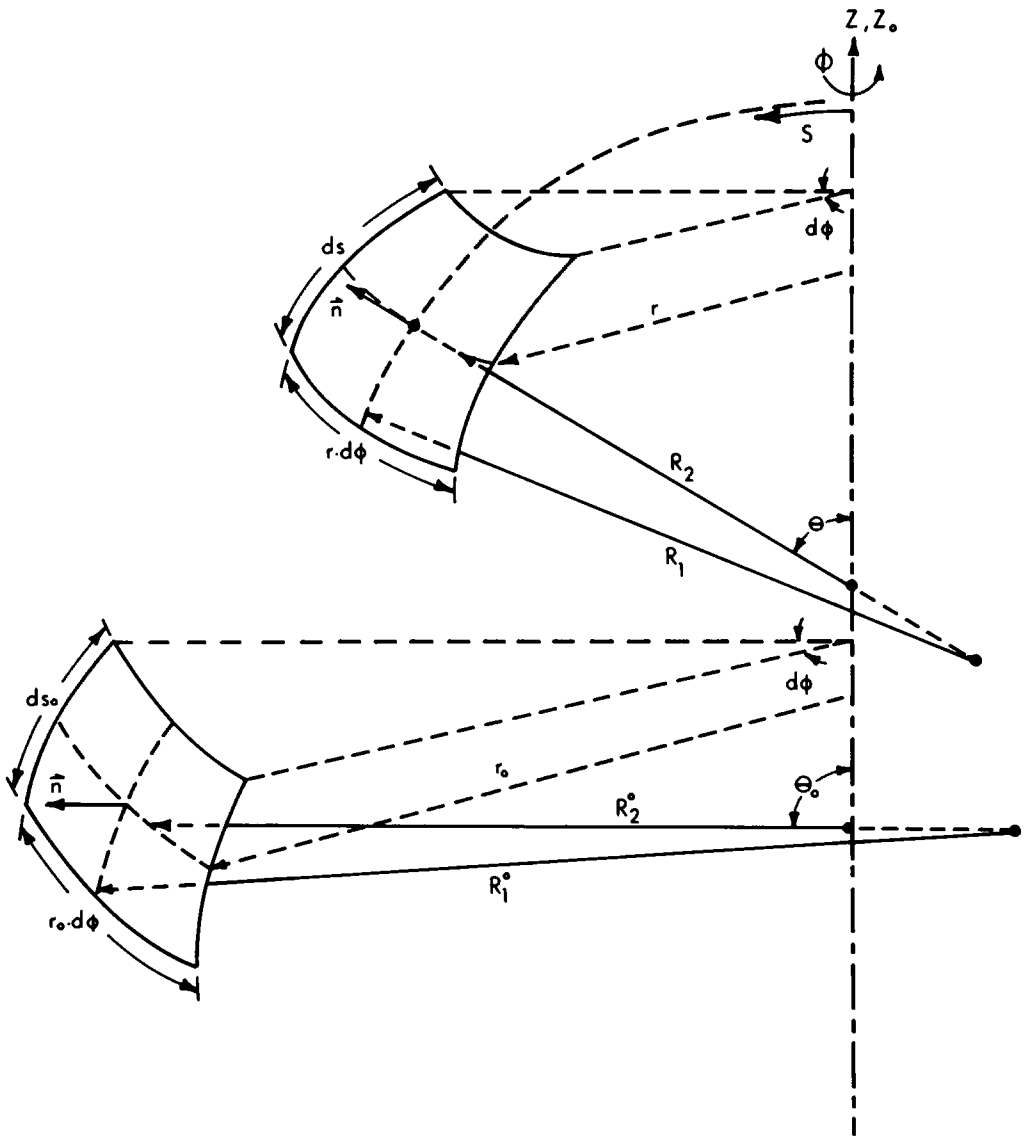

FIGURE 3 Illustration of the initial (undeformed) and final (deformed) geometries of a specific element of the axisymmetric membrane surface. The spatial coordinates are (r_0, z_0, ϕ) and (r, z, ϕ) for the initial and final states, respectively; the corresponding curvilinear coordinates are (s_0, θ_0, ϕ) and (s, θ, ϕ). The principal radii of curvature for the surface element are labeled (R_1^0, R_2^0) and (R_1, R_2); R_1 (or R_1^0) is the radius of curvature that describes a local arc of the surface meridian; R_2 (or R_2^0) describes a local arc of the surface in the plane which contains the surface normal and is orthogonal to the meridian contour.

where μ is the elastic shear modulus, B is the coefficient of local bending rigidity, Γ is a chemically-induced moment that can be caused by changes in the surface equilibrium, and $\bar{B}$ is the nonlocal coefficient of bending rigidity. The free energy per unit area (the integrand) is defined relative to the undeformed or initial state (area); for the constant area case, the initial and final (deformed) differential areas are equal, i.e., $dA_0 \equiv dA$. Of these material properties,

only the elastic shear modulus has been measured experimentally; the bending rigidity has been estimated from theoretical models which appear to correlate with meager experimental evidence (Evans and Hochmuth, 1978). No discriminatory data are available for separation of local and nonlocal bending effects. Local bending corresponds to a membrane material with rigidly connected layers of molecules which cannot slip relative to one another; nonlocal bending represents associated layers which can slip locally (e.g., a phospholipid bilayer where the terminal ends of acyl chains are unconnected). The difference between local and nonlocal bending energies is apparent when the variation of the free energy is taken,

$$\delta F = \int [\mu(\lambda - \lambda^{-3})\delta\lambda + (B \cdot K_1 + B \cdot K_2 + \Gamma + \overline{M})(\delta K_1 + \delta K_2)]\mathrm{d}A_0, \qquad (12)$$

where, $\overline{M} \equiv \overline{B} \int (K_1 + K_2)\mathrm{d}A_0$. Note that the integrand includes a parameter, $\overline{M}$, that is evaluated by the global integration of the mean curvature (a type of "global" bending moment), whereas the local bending moment, $B(K_1 + K_2)$, is involved in the integration over the contour. The physical significance is illustrated by bending a tablet of paper: if the sheets of paper are glued together, the extrinsic bending rigidity of the tablet is very large; whereas the tablet is very flexible if the sheets are unconnected.

The first and second variations are related to the first and second partial derivatives as previously discussed,

$$\delta F = \sum_{i=1}^{N} \frac{\partial F}{\partial a_i} \cdot \delta a_i,$$

$$\delta^2 F = \sum_{i=1}^{N} \sum_{j=1}^{N} \frac{\partial^2 F}{\partial a_i \partial a_j} \cdot \delta a_i \cdot \delta a_j.$$

With the elastic free energy functional, these are expressed as a set of integrals of partial derivatives,

$$\frac{\partial F}{\partial a_i} = \int \left[\mu(\lambda - \lambda^{-3}) \frac{\partial \lambda}{\partial a_i} + (B \cdot K_1 + B \cdot K_2 + \Gamma + \overline{M}) \left(\frac{\partial K_1}{\partial a_i} + \frac{\partial K_2}{\partial a_i}\right)\right] \mathrm{d}A_0, \qquad (13)$$

and

$$\frac{\partial^2 F}{\partial a_i \partial a_j} = \int \left\{\mu\left[(\lambda - \lambda^{-3}) \frac{\partial^2 \lambda}{\partial a_i \partial a_j} + (1 + 3\lambda^{-4}) \frac{\partial \lambda}{\partial a_i} \frac{\partial \lambda}{\partial a_j}\right] + (B \cdot K_1 + B \cdot K_2 + \Gamma + \overline{M}) \left(\frac{\partial^2 K_1}{\partial a_i \partial a_j} + \frac{\partial^2 K_2}{\partial a_i \partial a_j}\right) + B\left(\frac{\partial K_1}{\partial a_i} + \frac{\partial K_2}{\partial a_i}\right)\left(\frac{\partial K_1}{\partial a_j} + \frac{\partial K_2}{\partial a_j}\right) + \frac{\partial \overline{M}}{\partial a_j}\left(\frac{\partial K_1}{\partial a_i} + \frac{\partial K_2}{\partial a_i}\right)\right\} \mathrm{d}A_0, \qquad (14)$$

where,

$$\frac{\partial \overline{M}}{\partial a_j} = \overline{B} \int \left(\frac{\partial K_1}{\partial a_j} + \frac{\partial K_2}{\partial a_j}\right) \mathrm{d}A_0.$$

To evaluate the necessary partial derivatives in Eqs. 13 and 14 and to solve the system of equations, (11), for the minimum, the axisymmetric geometry will be defined in curvilinear

coordinates (s, θ, ϕ) and (s_0, θ_0, ϕ_0) for the final (deformed) and initial contours, respectively. The distance along the meridian (contour generator) is defined as s, the coordinate, θ, is defined as the angle between the outward normal to the surface and the axis of symmetry, and the coordinate, ϕ, is the azimuthal angle. Fig. 3 illustrates these coordinates for initial and deformed surface elements. The cylindrical coordinates (r, z) can be expressed as parametric functions of the coordinate, s. Likewise, for an axisymmetric surface, the angle, θ, can be expressed as a function of position along the meridian, $r = f(s)$, $z = f(s)$, $\theta = f(s)$, where,

$$\begin{aligned} dr/ds &= \cos\theta, \\ dz/ds &= -\sin\theta. \end{aligned} \tag{15}$$

The principle curvature changes of the surface are given by,

$$\begin{aligned} K_1 &= \frac{1}{R_1} - \frac{1}{R_1^0} = \frac{d\theta}{ds} - \frac{d\theta_0}{ds_0}, \\ K_2 &= \frac{1}{R_2} - \frac{1}{R_2^0} = \frac{\sin\theta}{r} - \frac{\sin\theta_0}{r_0}. \end{aligned} \tag{16}$$

The constant area restriction is explicitly satisfied by the relation,

$$r_0 \cdot ds_0 \equiv r \cdot ds, \tag{17}$$

where the subscript, 0, refers to the initial, undeformed surface geometry. The membrane extension ratio is defined by the ratio of differential lengths along meridians of the deformed and undeformed surfaces, $\lambda = ds/ds_0$; this specifies the planar deformation of the axisymmetric surface. Because of the constant area requirement, the membrane extension ratio is equivalently given by the ratio of radial coordinates for corresponding surface locations,

$$\lambda = r_0/r. \tag{18}$$

From differential relations for the initial and final surface geometries, the surface deformation and spatial coordinates of the final shape can be expressed in terms of the initial surface geometry which is presumed to be known,

$$\begin{aligned} \frac{dr}{ds} &= \frac{1}{\lambda}\frac{d}{ds_0}\left(\frac{r_0}{\lambda}\right) = \cos\theta, \\ \frac{d\lambda}{ds} &= (\lambda \cdot \cos\theta_0 - \lambda^3 \cdot \cos\theta)/r_0, \\ \frac{dz}{ds_0} &= -\lambda \cdot \sin\theta, \\ \theta &= f(s_0). \end{aligned} \tag{19}$$

The curvilinear coordinate, θ, as a function of surface position embodies the axisymmetric contour shape. A functional form for the angle, θ, is needed in terms of independent variables (a_i, s_0), which satisfies the necessary continuity conditions. For the membrane force resultants (tensions and transverse shear) to be continuous, the angle with its first and second derivatives must be continuous. It is possible to define a piecewise continuous polynomial in s_0 that

satisfies these criteria (Conte and deBoor, 1972); this is a sequence of fifth-order polynomials, each defined for a specific region (say the pth) by,

$$\theta_p(s_0) = \sum_{n=1}^{5} C_{pn}(s_0 - s_{0p})^n, \tag{20}$$

where,

$$\theta_p(s_{0p}) = \theta_{p-1}(s_{0p}),$$
$$\left.\frac{d\theta_p}{ds_0}\right|_{s_{0p}} = \left.\frac{d\theta_{p-1}}{ds_0}\right|_{s_{0p}},$$
$$\left.\frac{d^2\theta_p}{ds_0^2}\right|_{s_{0p}} = \left.\frac{d^2\theta_{p-1}}{ds_0^2}\right|_{s_{0p}},$$

and s_{0p} are the region boundaries for each polynomial of the sequence. The coefficients, C_{pn}, are linear combinations of a set of variables, a_i, given by,

$$a_i = \begin{cases} \theta(s_{0p}), \\ \left.\dfrac{d\theta}{ds_0}\right|_{s_0=0}, \left.\dfrac{d\theta}{ds_0}\right|_{s_0=s_{max}}. \\ \left.\dfrac{d^2\theta}{ds_0^2}\right|_{s_0=0}, \left.\dfrac{d^2\theta}{ds_0^2}\right|_{s_0=s_{max}} \end{cases} \tag{21}$$

The geometric variations involved in the free energy variations are given by a set of nonlinear differential equations,

$$\frac{d}{ds_0}\left(\frac{\partial\lambda}{\partial a_i}\right) = \left(\frac{\partial\lambda}{\partial a_i}\cdot\cos\theta_0 - 3\lambda^2\cdot\frac{\partial\lambda}{\partial a_i}\cdot\cos\theta + \lambda^3\cdot\sin\theta\cdot\frac{\partial\theta}{\partial a_i}\right)\Big/ r_0,$$
$$\frac{d}{ds_0}\left(\frac{\partial z}{\partial a_i}\right) = -\frac{\partial\lambda}{\partial a_i}\cdot\sin\theta - \lambda\cos\theta\cdot\frac{\partial\theta}{\partial a_i},$$
$$\frac{\partial K_1}{\partial a_i} = -\frac{1}{\lambda^2}\cdot\frac{\partial\lambda}{\partial a_i}\cdot\frac{d\theta}{ds_0} + \frac{1}{\lambda}\cdot\frac{d}{ds_0}\left(\frac{\partial\theta}{\partial a_i}\right),$$
$$\frac{\partial K_2}{\partial a_i} = \frac{1}{r_0}\cdot\frac{\partial\lambda}{\partial a_i}\cdot\sin\theta + \frac{\lambda}{r_0}\cdot\cos\theta\cdot\frac{\partial\theta}{\partial a_i}. \tag{22}$$

The second partial derivatives are similar differential equations. Geometric constraints and partial derivatives are illustrated by the particular relation for constant volume:

$$G = V_0 + \int z\cdot\cos\theta\cdot dA_0,$$
$$\frac{\partial G}{\partial a_i} = \int\left(\frac{\partial z}{\partial a_i}\cdot\cos\theta - z\sin\theta\cdot\frac{\partial\theta}{\partial a_i}\right)dA_0, \tag{23}$$

where V_0 is the cell volume. The partial derivatives of the coordinate, θ, with respect to the independent variables, a_i, are simply fixed matrices, which are determined by $\partial C_{pn}/\partial a_i$.

The procedure for obtaining a minimum energy contour is implemented by a computer algorithm based on the Newton-Raphson technique of successive approximations to the variables, a_i. The matrices, $\bar{F}_{ij}$ and $\bar{G}_{ki}$, and vectors, $\bar{F}_i$ and G_i, are evaluated with an initial "guess," $\bar{a}_i$; then successive "guesses," a_i, are obtained from the system of equations, (11), until the system convergence criteria are satisfied [e.g., $\Sigma_{i-1}^{N}|\bar{F}_i\bar{F}_i| + \Sigma_{i-1}^{N}|G_iG_i|$ or $\Sigma_{i-1}^{N}|(a_i - \bar{a}_i)(a_i - \bar{a}_i)|$ are small]. Eqs. 13, 14, 22, and 23 are integrated simultaneously to provide the required matrices and vectors used in Eq. 11. The system of equations usually involves no more than three free angles (with the angles at the ends fixed), two Lagrange multipliers (one for constant volume and the other for the fixed distance between pipets), plus the appropriate derivatives at the ends as free variables to give a dimensionality of (9 × 9).

RESULTS: MICROPIPET ASPIRATION

Micropipet aspiration of a flaccid red cell is shown in Fig. 1. The aspirated cell projection length exhibits a linear dependence on suction pressure like the sample data in Fig. 4 (taken from Waugh, 1977). Evans (1973) analyzed the experiment using an approximation of the surface as a flat sheet (since the membrane force resultants drop off inversely with the square of the distance from the pipet entrance); neglecting bending rigidity, this analysis yielded a linear relationship with a first-order elastic constitutive relation. Correlation of red cell aspiration data with the approximate analysis has provided a value for the elastic shear modulus of 6.6 × 10^{-3} dyn/cm at 25° (Waugh and Evans, 1979). Even though the observations have indicated that bending rigidity is small, no direct evaluation of bending effects has been previously undertaken for the aspiration experiment.

With the minimum energy method described here, the micropipet aspiration experiment has been modeled for a two order of magnitude range of bending-to-shear rigidity ratio, i.e., $\tilde{B} \equiv B/(\mu \cdot R_0^2) \sim 10^{-4}$–$10^{-2}$. For an elastic shear modulus of 6.6 × 10^{-3} dyn/cm and an outer radius of the initial cell cross section equal to 3.91 × 10^{-4} cm, the elastic bending modulus would vary between 10^{-13} and 10^{-11} ergs (dyn-cm) for the above range. The outer radius, R_0, is the value appropriate to the initial cell cross section shown in Fig. 5 *a* (taken from Evans and Fung, 1972). With this initial cross section and an intermediate value of 10^{-3} for $\tilde{B}$, Fig. 5 *b* is a minimum energy contour for an aspirated length to pipet radius ratio,

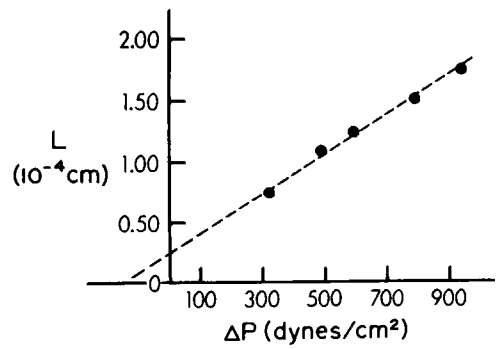

FIGURE 4 An example of data for micropipet aspiration of a flaccid cell (taken from Waugh, 1977). The suction pressure varies linearly with the length of the cell in the micropipet; the measurement was made with a 10^{-4}-cm diameter pipet.

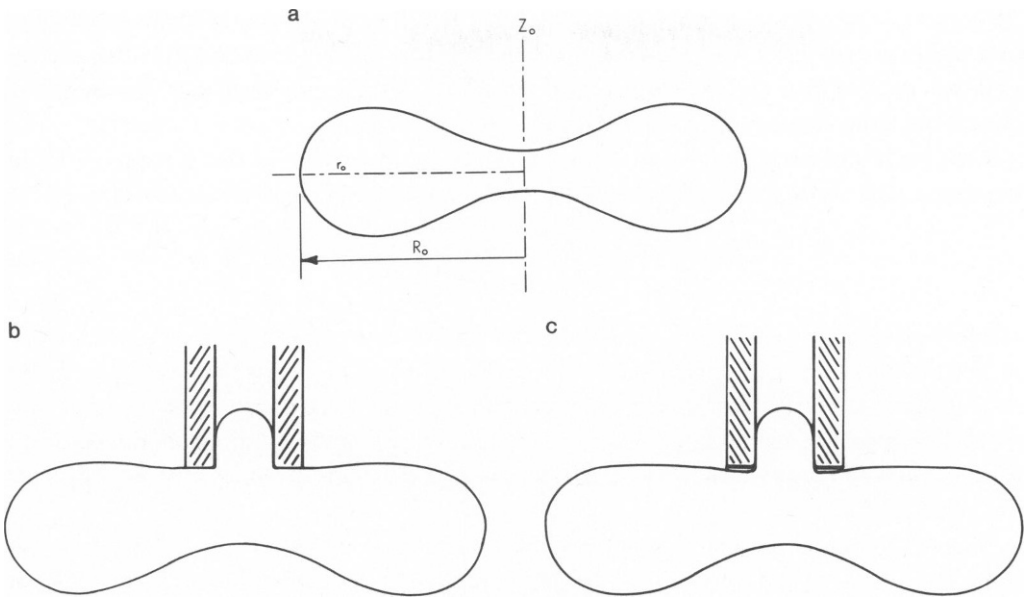

FIGURE 5 (*a*) The average cross section for red cells in isotonic medium (taken from Evans and Fung, 1972). The outer radius, R_0, determines the scale; its value is 3.91×10^{-4} cm. (*b*) Minimum energy contour for an aspirated length-to-pipet radius ratio of 2:1; the contour was required to lie along the pipet front face and inner wall. The bending-to-shear rigidity ratio, $\tilde{B}$, was 10^{-3}. (*c*) Minimum energy contour for the same aspirated length-to-pipet radius ratio as 5*b;* but the contour was only required to lie along the inner wall of the pipet and was totally unsupported outside. (It is important to note that the situation depicted here cannot be maintained unless the membrane is struck to the pipet wall; there is no force imparted to the membrane at the entrance to the pipet. However, this unrealistic case is very useful because it provides an upper limit for the bending energy contributed by the sharp corner where the membrane enters the mouth of the pipet.) The bending-to-shear rigidity ratio was the same value as that for 5*b*.

L/R_p, of 2:1 where the contour was required to lie along the pipet surface on the front face and inner wall as shown; this constraint is accomplished by setting the curvilinear coordinate, θ, equal to zero along the front face of the pipet and equal to $\pi/2$ along the inner wall. Since it was found that the shape of the projection cap inside the pipet had little influence on the total membrane free energy, the cap was defined to be a spherical segment for convenience. To assess the importance of the corner at the entrance to the inner cylinder of the pipet, an alternate pipet entrance condition was investigated for the contour which only required that the contour be constrained to the inner wall but was totally unsupported outside; Fig. 5 *c* is the minimum energy contour. (It is important to note that the situation depicted in Fig. 5 *c* cannot be maintained unless the membrane is stuck to the pipet wall; there is no force imparted to the membrane at the entrance to the pipet. However, the unrealistic case in Fig. 5 *c* is very useful because it provides an upper limit for the bending energy contributed by the sharp corner where the membrane enters the mouth of the pipet.) The total membrane free energy was different for the two different entrance conditions (illustrated in Figs. 5 *b* and *c*); however, the derivative of the free energy with respect to the aspirated length, which is the pipet suction pressure, was essentially the same for both conditions. Also, for the two order of magnitude range of bending-to-shear rigidities investigated, the radius of curvature of the membrane at

the corner of the pipet mouth was very small, such that the curvilinear coordinate, θ, went to zero within a very short distance from the corner. The radius of curvature for the contour meridian at the corner varied between 0.01 and 0.03 times the outer radius of the initial cell cross section; this range is equivalent to $0.04–0.12 \times 10^{-4}$ cm.

From Eq. 5, the pipet suction pressure is given by the derivative of the free energy of the membrane with respect to aspirated length; in a dimensionless form, this relationship is,

$$\frac{\Delta P \cdot R_p}{2\mu} = \frac{R_0^2}{2\pi R_p^2}\left(\frac{\partial \tilde{F}}{\partial \tilde{L}}\right), \tag{24}$$

where the free energy has been normalized by μR_0^2 and the cell projection length by R_p, and $\tilde{F} \equiv F/\mu R_0^2$, and $\tilde{L} \equiv L/R_p$. Eq. 24 is a dimensionless form of the approximate membrane tension local to the pipet entrance. For a pipet diameter of 1×10^{-4} cm, Fig. 6 contains plots of the dimensionless membrane tension versus the dimensionless cell projection length; the effect of bending rigidity is shown by the three curves which correspond to values of $\tilde{B}$ equal to 10^{-4}, 10^{-3}, and 10^{-2}.

Each of these curves begins at the origin; the dashed lines represent the linear extrapolation of the measurable data range. Because of the limitation of optical resolution, data cannot be obtained accurately for values of the projection length $< 0.5 \times 10^{-4}$ cm ($\tilde{L} = 1$). It is apparent, however, that the extrapolated intercept will correspond to a positive pressure if the value of $\tilde{B}$ exceeds 10^{-3}. As shown in Fig. 4, the extrapolated pressure intercept is negative,

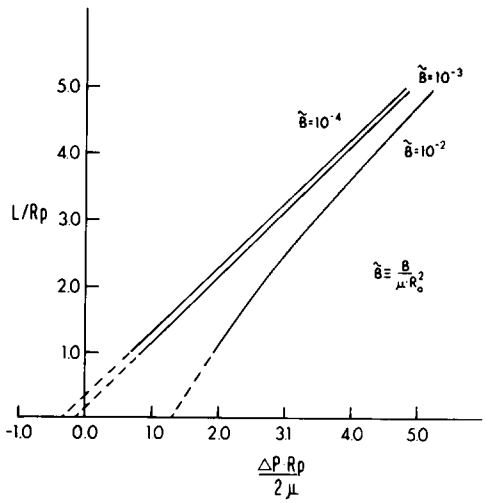

FIGURE 6 The results of aspirated length-to-pipet radius ratio versus the suction pressure times pipet radius, normalized by twice the elastic shear modulus. The dimensionless tension, $\Delta P \cdot R_p/2\mu$, is essentially a linear function of the aspirated length-to-pipet radius ratio. A two order of magnitude range of bending-to-shear rigidity ratio, $\tilde{B} = B/\mu \cdot R_0^2$, is represented by the three curves. For an elastic shear modulus of 6.6×10^{-3} dyn/cm, the elastic bending modulus would range between 10^{-13} and 10^{-11} dyn-cm (ergs). The dashed lines are linear extrapolations of the measurable data range. As shown in Fig. 4, the extrapolated pressure intercept for aspiration of a flaccid red cell is negative, which demonstrates that the upper bound for the bending modulus is 10^{-12} dyn-cm (ergs).

which demonstrates that the upper bound for $\tilde{B}$ would be 10^{-3} for the red cell membrane. Again, this value corresponds to a bending modulus of 10^{-12} dyn-cm (ergs) for a shear modulus of 6.6×10^{-3} dyn/cm. The slope of the dimensionless tension versus the dimensionless length provides the elastic shear modulus since the curves are nearly linear; the slopes of the two curves for $\tilde{B} = 10^{-4}$, 10^{-3} are about 10% less than the slope obtained from the approximate solution (Waugh and Evans, 1979). In addition, a twofold increase in pipet diameter (from 1×10^{-4} to 2×10^{-4} cm) has only a very slight effect on the slope (less than a few percent) and shifts the curves slightly to the left.

RESULTS: ASPIRATION FOLLOWED BY ADHESION

As shown in Figs. 1 and 2 *a*, a flaccid red cell is initially aspirated with a fixed suction pressure; then, it is moved close to a rigid "test" surface where adhesion will eventually take place. After adhesion occurs, a new equilibrium shape exists that includes a displacement of the cell projection in the pipet plus the adhesion of the outer cell envelope to the sphere. To model this problem, the distance between pipets becomes an additional constraint to be satisfied. The membrane is assumed to be tightly associated with the spherical surface over the contact region (no gaps); thus, the membrane contour is required to be tangent to the spherical surface at the end of the contact region.

Fig. 7 illustrates minimum energy contours for two specific contact areas where the initial state is shown in Fig. 5 *b*. The equilibrium cell length in the pipet is determined by Eq. 5 with the pressure fixed at the initial value, $(\partial F/\partial L)_{A_c} = \Delta P(\pi R_p^2)$, and the contact area fixed. Thus, there is a specific relation between cell length in the pipet and the contact area, i.e., $L = f(A_c)$. This relationship is illustrated in Fig. 8 for the particular pipet and cell arrangement shown in Figs. 7 *a* and *b*. (The contact area for a spherical "test" surface is a linear function of the height, Δz, of the polar cap that covers the spherical cell [shown in Fig. 7]. Since this is directly measureable in an experiment, the results in Figs. 8 and 9 are plotted versus Δz.) The interfacial free energy density, γ, associated with the work of adhesion is obtained with Eq. 6, $\gamma = (\partial F/\partial A_c)_{L=f(A_c)}$. Along the functional path, $L = f(A_c)$, the interfacial free energy density is the differential equation,

$$\gamma = \frac{dF}{dA_c} - \Delta P(\pi R_p^2) \cdot \frac{dL}{dA_c}. \tag{25}$$

For the particular pipet and cell arrangements shown in Fig. 7, the interfacial free energy density is plotted in Fig. 9 versus the height of the polar cap that covers the spherical cell. From Figs. 7 *b* and 9, it is observed that isotropic tension and internal pressure begin to dominate membrane conformation for interfacial energy densities in excess of 5×10^{-3} ergs/cm^2 (for an elastic shear modulus of 6.6×10^{-3} dyn/cm). It is apparent that only small displacements in the pipet occur until the pressure inside the cell is forced to increase; the pressure increases because the cytoplasm is incompressible and the volume is fixed. As evidenced by the rounded contour in Fig. 7 *b*, membrane tensions build up over the entire cell surface instead of being simply concentrated near the pipet or contact regions. Study of the differential equation, (Eq. 25), shows the rationale for the behavior observed in Fig. 8. When

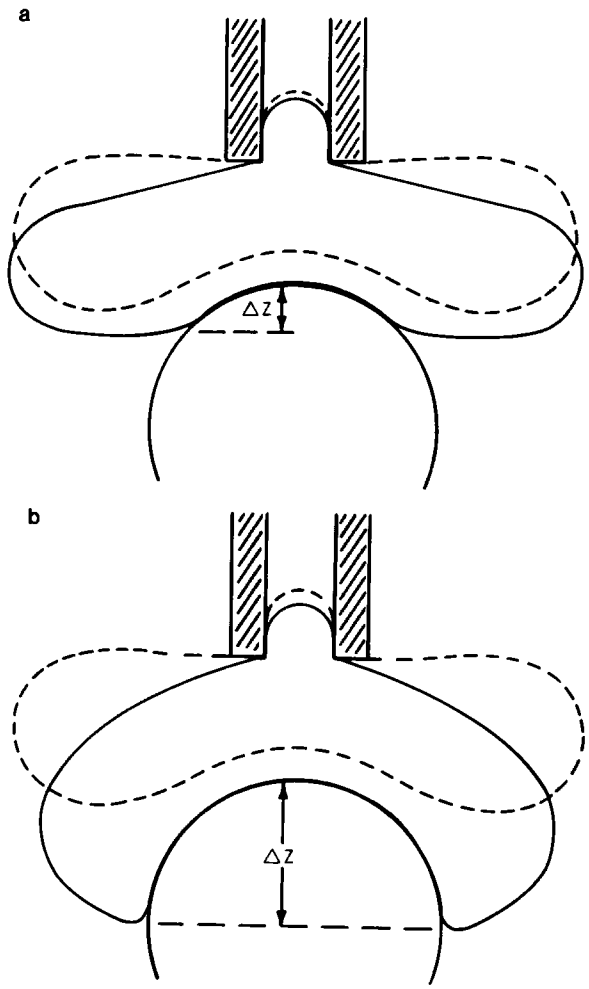

FIGURE 7 Minimum energy contours (solid lines) for two specific contact areas on the spherical cell surface; the initial state (dashed lines) before adhesion was taken as Fig. 5*b*. (The contours in 7*a* and *b* are calculated with a bending-to-shear rigidity ratio of $\tilde{B} = 10^{-3}$. The values of γ are scaled by the membrane elastic shear modulus.) Note in Fig. 7*b*, the internal pressure has forced the surface to "round-up" and displacement of the membrane projection in the pipet becomes appreciable. Fig. 7*a* corresponds to an interfacial free energy density for adhesion, γ, of 3×10^{-4} ergs/cm^2; by contrast, Fig. 7*b* corresponds to value for γ of 4×10^{-3} ergs/cm^2.

the membrane contour is rounded, little change in shape is possible; thus, the free energy change is small, e.g., $dF/dA_c \sim 0$, which leads to a direct relation between γ and ΔP,

$$-\left(\frac{dL}{dA_c}\right) \sim \frac{\gamma}{\Delta P(\pi R_p^2)}. \tag{26}$$

Eq. 26 is valid whenever the shear and bending elastic energies are negligible; for example, this is always the case for large phospholipid bilayer vesicles (with liquid acyl chains). For red cell adhesion, Eq. 26 is approached as the adhesive energy density, γ, exceeds the elastic shear modulus.

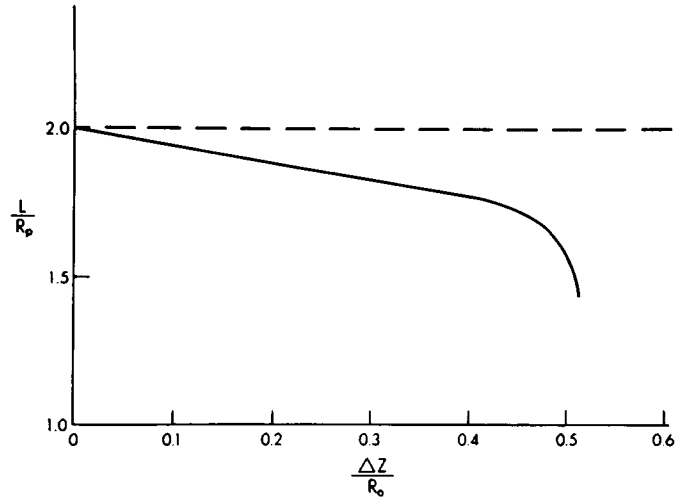

FIGURE 8 Aspirated projection length in the pipet versus the height of the polar cap that covers the spherical cell for the particular pipet and cell arrangement in Fig. 7.

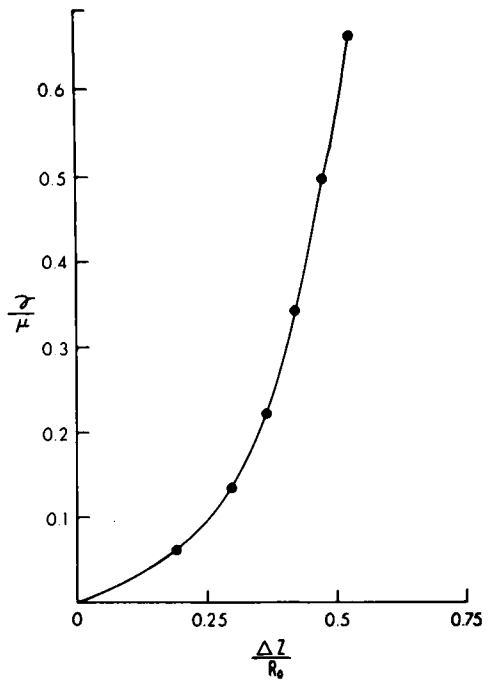

FIGURE 9 The interfacial free energy density, γ, for the work of adhesion versus the height of the polar cap that is produced by the adhesion. The ordinate scale is determined by the elastic shear modulus, μ, which has been measured to be 6.6×10^{-3} dyn/cm (Waugh and Evans, 1979).

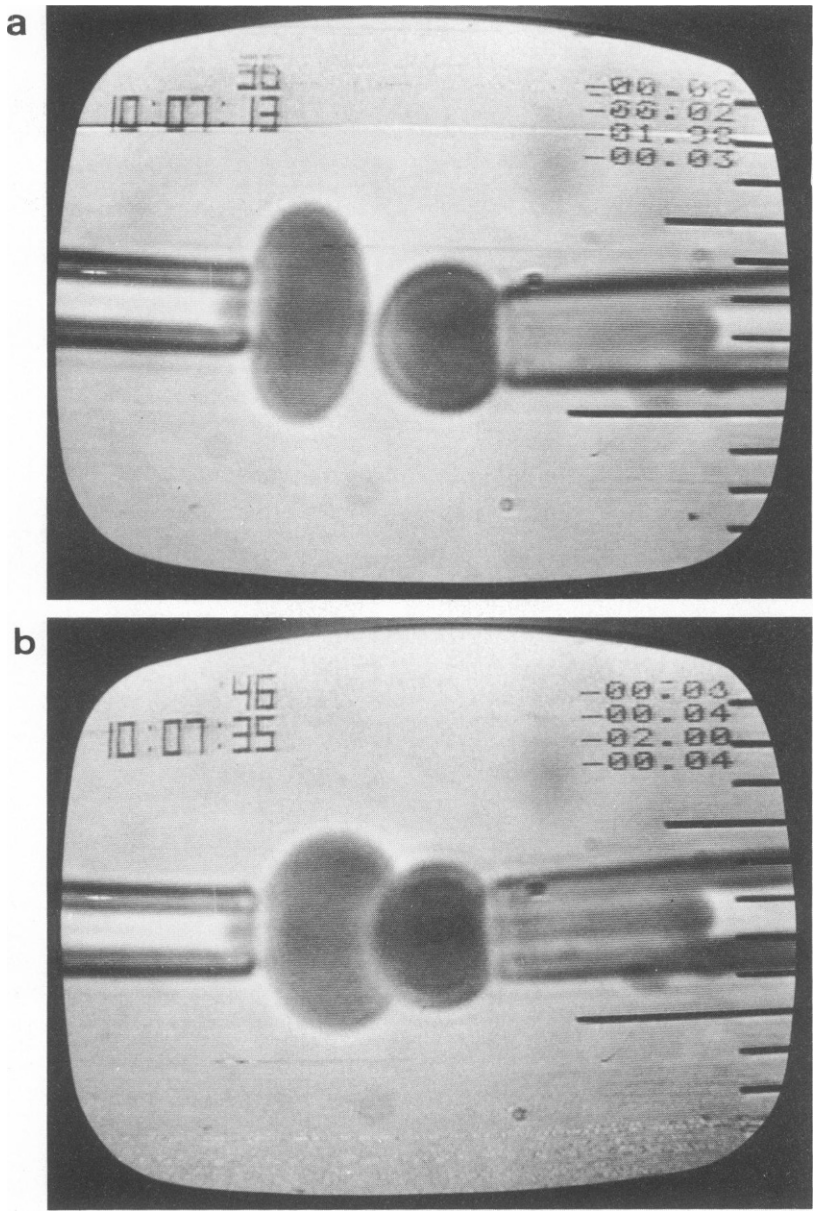

FIGURE 10 Photographs of videorecordings of an aspiration and adhesion experiment with an osmotically preswollen red cell.

These results suggest that preswollen red cells could be used with the advantage that there is no dimple region; Fig. 10 shows a particular experiment of this type. Fig. 11 illustrates the minimum energy contours for a preswollen form of the shape from Fig. 5 *a* (a 30% increase in volume) in a micropipet and after adhesion. For the range of interfacial energy densities from 5×10^{-3} to 5 ergs/cm^2, the deformed contour approaches an axisymmetric surface of constant mean curvature,

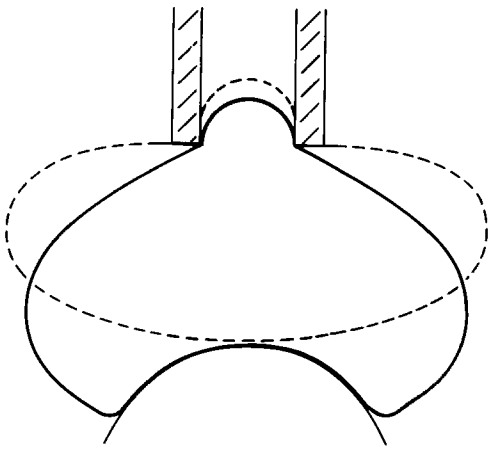

FIGURE 11 Minimum energy contours for a preswollen form of Fig. 5*a* (30% increase in volume). The dashed contour is the initial aspirated shape and the solid contour is the final shape after adhesion.

$$1/R_1 + 1/R_2 = \text{constant}; \tag{27}$$

this equation can be integrated to give an elliptic integral (Evans and Skalak, 1980). With the constant surface area and volume restriction plus Eq. 27, the relationship between cell projection length, L, and the contact area, A_c, can be directly determined. Hence, the interfacial free energy density is approximated by Eq. 26 and is directly related to the pipet suction force.

CONCLUSIONS

From the analysis of micropipet aspiration of a flaccid red cell, the conclusions are that the bending rigidity of the membrane does not significantly influence the suction pressure over the observable range of cell projection lengths and that the simple analysis for aspiration of a "flat" membrane surface (Evans, 1973; Waugh and Evans, 1979) is a good approximation. The experimental data show that the upper bound for the bending or curvature elastic modulus of the red cell membrane is 10^{-12} ergs (dyn-cm), which agrees with previous theoretical derivations (Evans and Hochmuth, 1978; Evans and Skalak, 1980).

The study of red cell adhesion shows that the shape change of the cell contour can be used to evaluate the interfacial free energy density for adhesion in the range of 10^{-4} to 5×10^{-3} ergs/cm^2. For interfacial energies in excess of the surface shear modulus and up to the membrane tension for lysis (~5–10 dyn/cm), the pipet suction pressure and displacement of the aspirated cell projection are used to establish the interfacial free energy density. For example, preliminary experiments have shown that adhesion which is mediated by high molecular weight dextran (~150,000 mol wt, concentrations of 1–3 gm %) in buffered isotonic saline (~150 mM) is represented by interfacial free energy densities in the range of 5×10^{-4} to 5×10^{-3} ergs/cm^2. On the other hand, adhesion processes which are promoted by multivalent ligands clearly are characterized by interfacial free energy densities which can even exceed the upper bound set by the tension at lysis.

The assistance of Karen Buxbaum, who performed the adhesion experiments, is appreciated. The author acknowledges the helpful discussion with his colleague Robert Hochmuth.

Dr. Evans is supported by U.S. Public Health Service National Institutes of Health (NIH) Research Career Development Award HL00063. In addition, this work was supported in part by NIH grants HL16711 and HL24796.

Received for publication 10 October 1979 and in revised form 15 January 1980.

REFERENCES

BELL, G. I. 1979. A theoretical model for adhesion between cells mediated by multivalent ligands. *Cell Biophys.* **1**:133–147.

BROOKS, D. E. 1973. The effect of neutral polymers on the electrokinetic potential of cells and other charged particles. III. Experimental studies on the dextran/erythrocyte system. *J. Colloid Interface Sci.* **43**:700–713.

CHIEN, S. 1975. Biophysical behavior of red cells in suspensions. *In* The Red Cell. Vol. II. 2nd ed. D. M. Surgenor, editor. Academic Press, Inc., New York. 1031–1131.

CONTE, S. D., and C. DEBOOR. 1972. Elementary Numerical Analysis. McGraw Hill Book Company, New York. 191–273.

COURANT, R., and D. HILBERT. 1966. Methods of Mathematical Physics. John Wiley & Sons, Inc., New York. Vol. 1. 164–274.

EVANS, E. A. 1973. New membrane concept applied to the analysis of fluid shear- and micropipette-deformed red blood cells. *Biophys. J.* **13**:941–953.

EVANS, E. A. 1974. Bending resistance and chemically induced moments in membrane bilayers. *Biophys. J.* **14**:923–931.

EVANS, E., and Y. C. FUNG. 1972. Improved measurements of the erythrocyte geometry. *Microvasc. Res.* **4**:335–347.

EVANS, E. A., and R. M. HOCHMUTH. 1978. Mechano-chemical properties of membranes. *In* Current Topics in Membranes and Transport. Vol. X. Kleinzeller and Bronner, editors. Academic Press, Inc., New York. 1–64.

EVANS, E. A., and R. SKALAK. 1980. Mechanics and Thermodynamics of Biomembranes. CRC. Press, West Palm Beach, Fla. In press.

ISRAELACHVILLI, J. N. 1974. Van der Waals forces in biological systems. *Q. Rev. Biophys.* **6**:341–387.

JENKINS, J. T. 1977. Static equilibrium configurations of a model red blood cell. *J. Math. Biol.* **4**:149–169.

NICHOLSON, G. L. 1974. The interactions of lectins with animal cell surfaces. *Int. Rev. Cytol.* **39**:89–190.

PARSEGIAN, V. A. 1975. Long range Van der Waals forces. *In* Physical Chemistry: Enriching Topics from Colloid and Surface Science. H. van Olphen and K. J. Mysels, editors. Theorex, La Jolla. 27–72.

SKALAK, R., P. R. ZARDA, K-M. JAN, and S. CHIEN. 1977. Theory of rouleau formation. *INSERM-Euromech 92 Proc.* **71**:299–308.

WAUGH, R. E. 1977. Temperature dependence of the elastic properties of red blood cell membrane. Doctoral dissertation, Duke University, Durham.

WAUGH, R., and E. A. EVANS. 1979. Thermoelasticity of red blood cell membrane. *Biophys. J.* **26**:115–132.

ZARDA, P. R., S. CHIEN, and R. SKALAK. 1977. Elastic deformations of red blood cells. *J. Biomech.* **10**:211–221.